Very-long-chain fatty acid sphingomyelin in nuclear lipid microdomains of hepatocytes and hepatoma cells: can the exchange from C24:0 to C16:0 affect signal proteins and vitamin D receptor?

Andrea Lazzarini[a], Antonio Macchiarulo[b], Alessandro Floridi[a], Alice Coletti[b], Samuela Cataldi[b], Michela Codini[b], Remo Lazzarini[a], Elisa Bartoccini[a], Giacomo Cascianelli[a], Francesco Saverio Ambesi-Impiombato[c], Tommaso Beccari[c], Francesco Curcio[c], and Elisabetta Albi[a]

[a]Laboratory of Nuclear Lipid BioPathology, CRABiON, 06100 Perugia, Italy; [b]Department of Pharmaceutical Science, University of Perugia, 06123 Perugia, Italy; [c]Department of Clinical and Biological Sciences, University of Udine, 33100 Udine, Italy

ABSTRACT **Lipid microdomains localized in the inner nuclear membrane are considered platforms for active chromatin anchoring. Stimuli such as surgery, vitamin D, or glucocorticoid drugs influence their gene expression, DNA duplication, and RNA synthesis. In this study, we used ultrafast liquid chromatography–tandem mass spectrometry to identify sphingomyelin (SM) species coupled with immunoblot analysis to comprehensively map differences in nuclear lipid microdomains (NLMs) purified from hepatocytes and hepatoma cells. We showed that NLMs lost saturated very-long-chain fatty acid (FA; C24:0) SM in cancer cells and became enriched in long-chain FA (C16:0) SM. We also found that signaling proteins, such as STAT3, Raf1, and PKCζ, were increased and vitamin D receptor was reduced in cancer cells. Because recent researches showed a shift in sphingolipid composition from C24:0 to C16:0 in relation to cell life, we performed a comparative analysis of properties among C16:0 SM, C24:0 SM, and cholesterol. Our results led us to hypothesize that the enrichment of C16:0 SM could determine enhanced dynamic properties of NLMs in cancer cells with an increased shuttling of protein signaling molecules.**

Monitoring Editor
Patricia Bassereau
Institut Curie

Received: Feb 10, 2015
Revised: May 1, 2015
Accepted: May 6, 2015

INTRODUCTION

Sphingomyelin (SM) was described as a dominant sphingolipid in mammalian cell membranes indispensable for cell function (Taniguchi and Okazaki, 2014). It contains acyl chains that vary in length from long-chain fatty acids (LCFAs), such as C16:0 palmitic acid, to very-long-chain fatty acids (VLCFAs) with 20 or more carbons, including saturated fatty acids (FAs) such as 20:0 arachidic acid, 22:0 behenic acid, 24:0 lignoceric acid, and mono- and poli-VLCFAs (Ohno *et al.*, 2010). VLCFAs are produced from certain LCFAs, provided through the diet or generated by FA synthase and elongated by FA elongase (Soupene and Kuypers, 2008).

SM and cholesterol (CHO) formed functional nanoscale-ordered domains, characteristic in particular of the external leaflet of cell membranes, whose thickness increased with the length of the acyl chain of SM (Róg and Vattulainen, 2014). Although a high-affinity interaction between SM and CHO was suggested (Radhakrishnan *et al.*, 2000; Li *et al.*, 2001), no compelling experimental evidence for the molecular basis of such a specific interaction has been reported in the literature, suggesting that the driving force for the formation of the lipidic domains is provided by the hydrophobic matching condition in membranes (Holopainen *et al.*, 2004).

This article was published online ahead of print in MBoC in Press (http://www.molbiolcell.org/cgi/doi/10.1091/mbc.E15-02-0071) on May 13, 2015.

Address correspondence to: Elisabetta Albi (elisabetta.albi@yahoo.com).

Abbreviations used: BSA, bovine serum albumin; CHO, cholesterol; Chr, chromatin; DTT, dithiothreitol; FBS, fetal bovine serum; H, hepatocyte; H35, H35 hepatoma cells; LCFA, long-chain fatty acid; NLM, nuclear lipid microdomain; NLR, nuclear lipid rafts; NM, nuclear membrane; NMx, nuclear matrix; PC, phosphatidylcholine; PKCζ, protein kinase Cζ; PMSF, phenylmethylsulfonylfluoride; SM, sphingomyelin; STAT-3, signal transducer and activator of transcription 3; VDR, vitamin D receptor; VLCFA, very-long-chain fatty acids.

However, it should be mentioned that interactions between SM and CHO were computationally studied in binary mixtures of CHO and SM via molecular dynamic simulation, with a focus on hydrogen bonding by showing that CHO formed more hydrogen bonds with SM than it formed with phosphatidylcholine (PC; Róg and Pasenkiewicz-Gierula, 2006). The studies on interactions among atoms of Aittoniemi *et al.* (2007) indicated that hydrogen bonding alone could not explain the higher affinity of CHO for SM but that one must also consider the contributions of van der Waals interactions between CHO and the choline groups of SM. In addition, CHO preferred saturated SM, with ordered acyl chains, to establish more favourable entropic interactions, since CHO might increase local entropy, and its interactions with disordered acyl chains in unsaturated phospholipids would lead to an ordering effect of CHO on acyl chains, thereby decreasing the local entropy (Slotte, 2013a). Measurements of sterol bilayer affinity demonstrated that palmitoyl SM was the optimal SM analogue for CHO (Slotte, 2013b). X-ray scattering data showed that 22:0, 23:0, and 24:0 SM included in a bilayer can lead to transbilayer interdigitation, that is, the distal part of a long acyl chain from a SM molecule in one leaflet penetrates into the opposing leaflet (Levin *et al.*, 1985). CHO and SM are present in membranes as lipid microdomains called lipid rafts, extracted as liquid ordered–phase detergent-resistant membranes whose functional role has long been subject of discussion in the membrane biophysics community. Brown (2006) claimed that the detergent-resistant membrane fractions did not represent lipid rafts present in the cells before extraction, even if raft-targeting signals identified by detergent-resistant membrane analysis were often required for protein function. Frisz *et al.* (2013) demonstrated that sphingolipid domains in the plasma membranes of fibroblasts did not contain CHO but that the latest affected the sphingolipid organization via an indirect mechanism that involved the cytoskeleton. Then Honigmann *et al.* (2014) proposed that alternative interactions were responsible for the strong local trapping of sphingolipid analogue in living nonstimulated cells. However, Mollinedo and Gajate (2015) demonstrated that lipid rafts behaved in cell membranes as major modulators of membrane geometry and lateral movement of molecules and as a platform for traffic and signal transduction proteins. In addition, lipid rafts represented the major platforms for signaling regulation in cancer (Mollinedo and Gajate, 2015).

We have previously demonstrated that lipid microdomains, rich in SM and CHO, are present in the inner nuclear membrane (NM), and we called these nuclear lipid microdomains (NLMs). They played different roles in relation to cell function by acting as platform for vitamin D receptor (VDR) in embryonic hippocampal cells (Bartoccini *et al.*, 2011) and for glucorticoid drugs in non-Hodgkin's T-cell human lymphoblastic lymphoma (Cataldi *et al.*, 2014). In the liver, NLMs acted as a resting place for active chromatin (Chr) and transcription factors by regulating DNA (Albi *et al.*, 2013) and RNA (Cascianelli *et al.*, 2008; Albi and Villani, 2009) synthesis. No data have existed until now about the SM FA species in NLMs.

Recent research on sphingolipid FAs has been focused on their role in cell physiopathology. Sassa *et al.* (2012) described that a shift in sphingolipid composition from C24:0 to C16:0 increased susceptibility to apoptosis in HeLa cells. The role of C16:0 had already been suggested by a study of Zhang *et al.* (2004) demonstrating that C16:0 induced apoptosis in human hepatoma HepG2 cells.

Hepatoma is a leading primary malignancy of the liver, one of the most common cancers worldwide. New therapeutic strategies targeted anti-signal transducer and activator of transcription 3 (STAT3) protein, a key regulator of inflammation, cell survival, and tumorigenesis of liver cells (Hung *et al.*, 2014), and Raf1, which prolongs cell survival and leads to cancer, even in the absence of oncogenic mutations (Gauthier and Mitchell, 2013). Protein kinase Cζ (PKCζ) was involved in the hepatocarcinogenic mechanism by controlling glycogen synthase kinase-3β (Desbois-Mouthon *et al.*, 2002). PKCζ stimulates and vitamin D inhibits hepatocellular carcinoma development (Guo *et al.*, 2013).

To address the role of SM present in NLMs on cell function, we examined the presence of SM species in NLMs purified from hepatocytes (H) and H35 hepatoma cells (H35) in relation to signal proteins and vitamin D3 receptor (VDR).

RESULTS

Nuclear rafts of hepatocytes and hepatoma cells

Highly purified H and H35 nuclei were used to prepare NLMs. The purification level of the nuclear preparation was similar to that previously reported (Cascianelli *et al.*, 2008). In the nuclei, after Barnes treatment, the activity of glucose-6-phosphatase was 7 ± 2 nmol/mg protein/min (H) and 6 ± 2 nmol/mg protein/min (H35). The NADH–cytochrome *c* reductase activity was undetectable in both preparations. The NLM fraction was obtained from triton solubilization. In H NLMs, the level of protein was 29.40 ± 2.21 µg/g liver, and in H35 NLMs, it was 1.31 ± 0.02 µg/106 cells, according to Cascianelli *et al.* (2008) and Bartoccini *et al.* (2011), respectively. No activity of glucose-6-phosphatase and NADH–cytochrome *c* reductase was detected in both preparations, indicating the absence of cytoplasmic contamination. These data were strongly supported by immunoblot analysis with giantin antibodies, a marker protein for Golgi membrane. The results showed that the band for giantin corresponding to an apparent molecular weight of 367 kDa was absent in H NLMs and H35 NLMs (Figure 1). The presence of STAT3, which is a marker of NLMs, demonstrates the purification of NLMs (Cascianelli *et al.*, 2008) (Figure 1a), although it was expressed 3.43 times in H35 NLMs in comparison with H NLMs (Figure 1b). For highlighting the level of NLM purification and to exclude possible Chr and nuclear matrix (NMx) contamination, lamin B was analyzed as marker of NLMs, whereas Chr and NMx were used as controls. In samples prepared from both H and H35 nuclei, the results showed the absence of lamin B in NMx and the very low level of protein in Chr, indicated by the possible presence of small parts of inner NM in the sample, and a higher protein content in NLMs, as previously reported (Cascianelli *et al.*, 2008; Figure 2). The level of CHO was 13.40 ± 0.22 µg/mg protein in H NLMs and 14.65 ± 0.38 µg/mg protein in H35 NLMs, similar to what was previously reported (Cascianelli *et al.*, 2008; Bartoccini *et al.*, 2011).

24:0 SM shifts to 16:0 SM in nuclear lipid rafts (NLRs) of cancer cells

We analyzed SM species in NLMs by using 16:0 SM, 18:1 SM, and 24:0 SM external calibrators; the results were compared with those of total NM. The results highlighted that, in NLMs prepared from cancer cells, the value of 16:0 SM increased 6.5 times and that of 24:0 SM decreased 18.65 times in comparison with NLMs from normal cells (Figure 3a). In NM, 16:0 SM increased 1.29 times and 24:0 SM decreased 4.6 times (Figure 3a). As NM contained NLMs, it is possible that the low variations present in NM reflected the changes observed in NLMs. To have a deeper insight of SM species containing saturated or unsaturated FAs, we evaluated the areas of all the peaks identified on the basis of their molecular weights and we analyzed their values in relation to protein content. A total of 24 species were investigated: 16:1 SM, 18:0 SM, 18:2 SM, 20:0 SM, 20:1 SM, 20:2 SM, 20:3 SM, 22:0 SM, 22:1 SM, 22:2 SM, 22:3 SM, 22:4 SM, 24:1 SM, 24:2 SM, 24:3 SM, 24:4 SM, 24:5 SM, 26:0 SM, 26:1 SM,

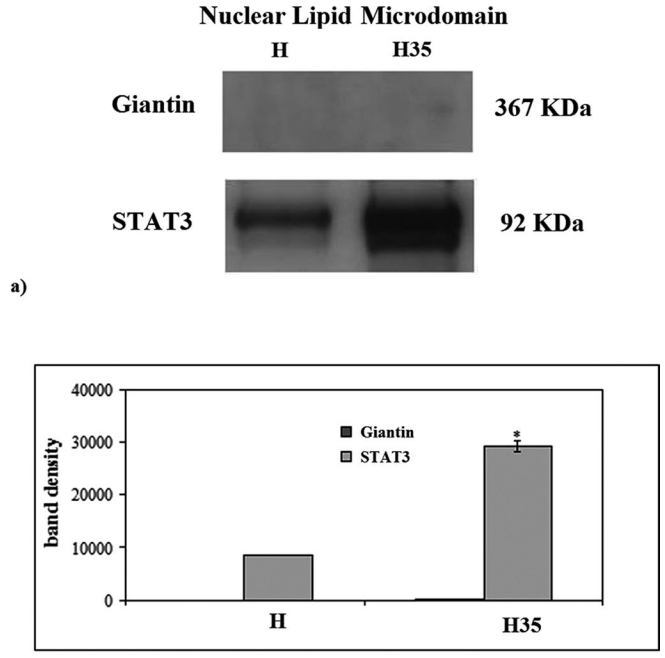

FIGURE 1: Giantin and STAT3 in NLMs purified from hepatocytes and hepatoma cells. (a) Immunoblot of proteins probed with specific antibodies. The position of giantin and STAT3 was indicated in relation to the position of molecular size standards. (b) The area density evaluated by densitometry scanning and analysis with Scion Image; the data represent the mean ± SD of three separate experiments. H, hepatocyte; H35, hepatoma cell line. *, $p < 0.001$ vs. H.

26:2 SM, 26:3 SM, 26:4 SM, 26:5 SM, 26:6 SM. Seven peaks were detected (Figure 3b). Significant differences in the levels of various lipid molecular species were found between H NLMs and H35 NLMs. H NLMs were richer in 20:0 SM content than H35 NLMs, and H35 NLMs were richer in 22:0 SM, 22:1 SM, 22:2 SM, 24:1 SM, 24:2 SM, and 24:4 SM content than H NLMs. In the intermediate-length acyl chains (20:0 and 22:0), there was an opposite effect to that observed for 16:0 and 24:0. However, 20:0 decreased 3.72 times and 22: 0 increased 2.07 times, similar to other FAs. Thus we focused our attention on FAs with higher variations, such as 16: 0 and 24:0. In NM, the changes in SM content between normal and cancer cells were not statistically significant. It is possible that the variations observed in NLMs were not high enough to effect changes in the total NM. We then compared the changes in the total levels of SM species containing saturated and unsaturated FAs. As reported in Figure 3c, the SM saturated FAs were 1.77 times lower and SM unsaturated FAs were 2.42 times higher in NLMs of cancer cells than in NLMs of normal cells. Thus the saturated/unsaturated FA ratio was 0.71 in H NLMs and 0.17 in H35 NLMs. Among unsaturated FAs, the monounsaturated FAs increased 3.10 times (22:1 SM) and 3.89 (24:1 SM), the di-unsaturated and tetra-unsaturated FAs increased in a range between 2.16 and 2.42. No significant changes were seen in NM (Figure 3c). To verify the specificity of SM changes, we analyzed PC and ceramide species by using 16:0 18:1 PC, 16:0 24:0 PC, 18:1 18:0 PC, 16:0 ceramide, 20:0 ceramide, and 24:0 ceramide as external calibrators. When the total SM species (Figure 3a) was compared with the total PC species (Figure 4a), it could be seen that PC was ~23 times higher than SM in NM, whereas both lipids had similar value in NLMs, as previously reported (Cascianelli *et al.*, 2008). The results showed no changes of PC species in both NM and NLMs prepared from normal and cancer cells (Figure 4a). Also, no changes were present in ceramide species in NM, whereas 16:0 ceramide decreased 1.5 times and 24:0 ceramide increased 3.13 times in NLMs (Figure 4b). It is possible that the variations of ceramide species were the results of the changes of substrates for sphingomyelinase, such as SM 16:0 and SM 24:0 (Figure 3a).

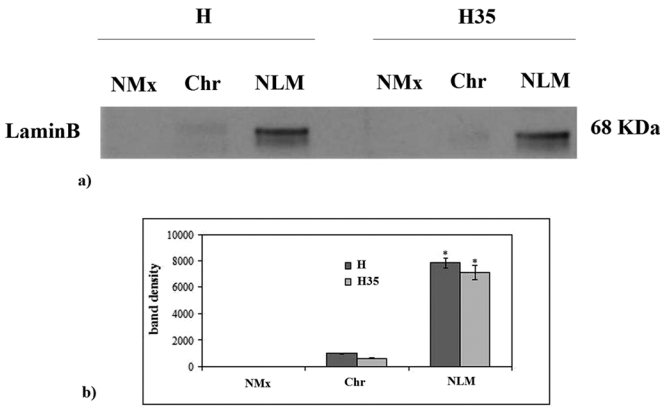

FIGURE 2: Lamin B in NMx, Chr, and NLM from hepatocytes and hepatoma cells. (a) Immunoblot of protein probed with specific antibody. The position of lamin B was indicated in relation to the position of the molecular size standard. (b) The area density evaluated by densitometry scanning and analysis with Scion Image; the data represent the mean ± SD of three separate experiments. H, hepatocyte; H35, hepatoma cell line. *, $p < 0.001$ vs. NMx and Chr.

Comparative analysis of properties among C16:0 SM, C24:0 SM, and CHO

To understand the possible meaning of the FA change in NLM SM of cancer cells, we studied the properties of C16:0 SM, C24:0 SM, and CHO, using molecular modeling calculations. Accordingly, tridimensional models of C16:0 SM, C24:0 SM, and CHO were generated in silico as detailed in the *Materials and Methods*. These models were instrumental in calculating surface descriptors, such as the polar surface area (Å^2) and total van der Waals surface area (Å^2), and geometrical descriptors, including the topological radius (Å) and topological diameter (Å). Specifically, the topological radius and diameter are respectively defined as the minimum vertex and the maximum vertex of a molecular graph representing the molecule, thereby providing the dimensions of the lipid (Todeschini *et al.*, 2000).

Based on our results, 16:0 SM (Figure 5a) is composed of a PC headgroup, a sphingosine moiety of 18 carbon atoms, and an N-linked FA chain of 16 saturated carbon atoms. Its polar surface area is 118 Å2, representing 10% of the total van der Waals surface area (1173 Å2). The topological radius of 16:0 SM is 17 Å, whereas the topological diameter is 33 Å. We found that 24:0 SM (Figure 5b) contains a PC headgroup, a sphingosine moiety of 18 carbon atoms, and an N-linked FA chain of 24 saturated carbon atoms. Its polar surface area is also 118 Å2, representing 8.5% of the total van der Waals surface area (1384 Å2) of the lipid. The topological radius of 24:0 SM is 21 Å, whereas the topological diameter is 41 Å. CHO (Figure 5c) is composed of a steroid nucleus with a polar hydroxyl group at C3 and a lipophilic side chain. Its polar surface area is 20 Å2, representing 3% of the total van der Waals surface area (607 Å2) of the lipid. The topological radius of CHO is 8 Å, whereas its topological diameter is 15 Å.

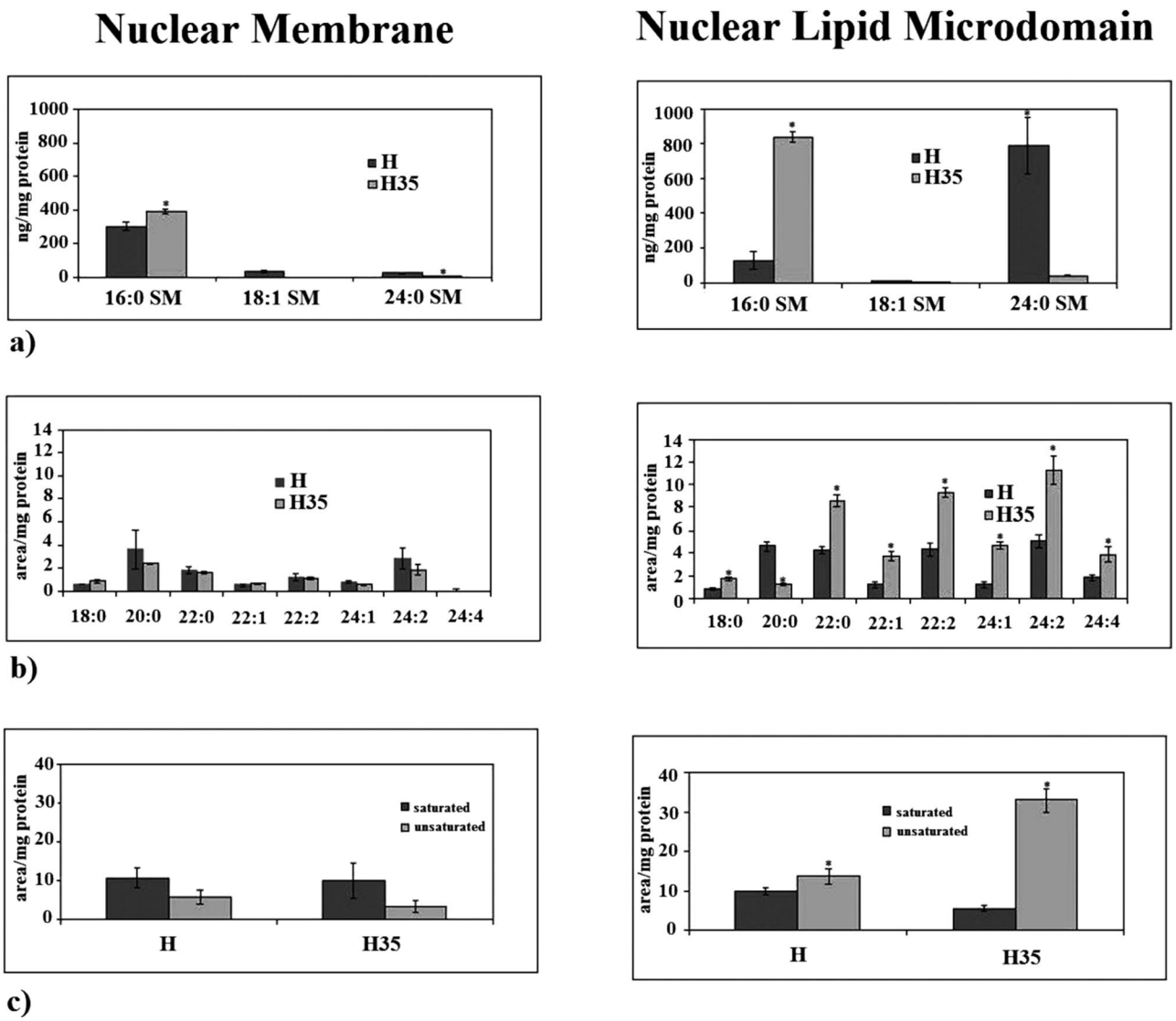

FIGURE 3: SM in NM and NLMs purified from hepatocytes and hepatoma cells. (a) SM species studied by using 16:0 SM, 18:1 SM, and 24:0 SM external calibrators. Data are expressed as nmol/mg protein and represent the mean ± SD of three separate experiments. (b) SM species studied by evaluating the areas of all the peaks identified on the basis of their molecular weight. Data are expressed as area/mg protein and represent the mean ± SD of three separate experiments. (c) Total saturated and unsaturated FAs. Data are expressed as area/mg protein and represent the mean ± SD of three separate experiments. H, hepatocyte; H35, hepatoma cell line. *, $p < 0.001$ vs. H.

Membrane thickness values are reported in the literature for 18:0 SM (46–47 Å) and 24:0 SM (52–56 Å) (Maulik and Shipley, 1995, 1996). Because membrane thickness is related to lipid chain length, we compared the topological diameter of lipids taken as a value of lipid chain length to infer the thickness of lipid rafts formed by 16:0 SM and 24:0 SM. This approximation resulted in a range of thickness values of 43–44 Å for the membrane composed of 16:0 SM and of 52–56 Å for the membrane composed of 24:0 SM in combination with CHO.

Signal proteins and VDR located in NLRs are different between hepatocytes and hepatoma cells

We have tested the possibility that the changes of SM species between H NMs and H35 NMs might be associated with variations of functional protein content. Raf1, PKCζ, and VDR expression have been analyzed by immunoblotting with specific antibodies in whole cells and in NLMs. Both samples showed immunoreactivity in correspondence to the bands with apparent molecular weights corresponding to 80 kDa (Raf1), 78 kDa (PKCζ), and 50 kDa (VDR) (Figure 6a). In whole cells, the band density increased 1.15 and 1.89 times for Raf1 and PKCζ, respectively, and decreased 1.92 times for VDR in cancer cells in comparison with normal cells. An increase of band density of 1.69 and 2.39 times for Raf1 and PKCζ, respectively, and a decrease of 2.87 times for VDR appeared in H35 NLMs in comparison with H NLMs (Figure 6b).

DISCUSSION

Considerable evidence suggests the implication of sphingolipids in cancer (Adan-Gokbulut *et al.*, 2013). Nowadays, researchers focus attention on the different species of sphingolipid molecules containing long and very long FAs. In has been demonstrated that cancer cells incorporate and remodel exogenous 16:0 into structural and oncogenic glycerophospholipids, sphingolipids, and ether lipids

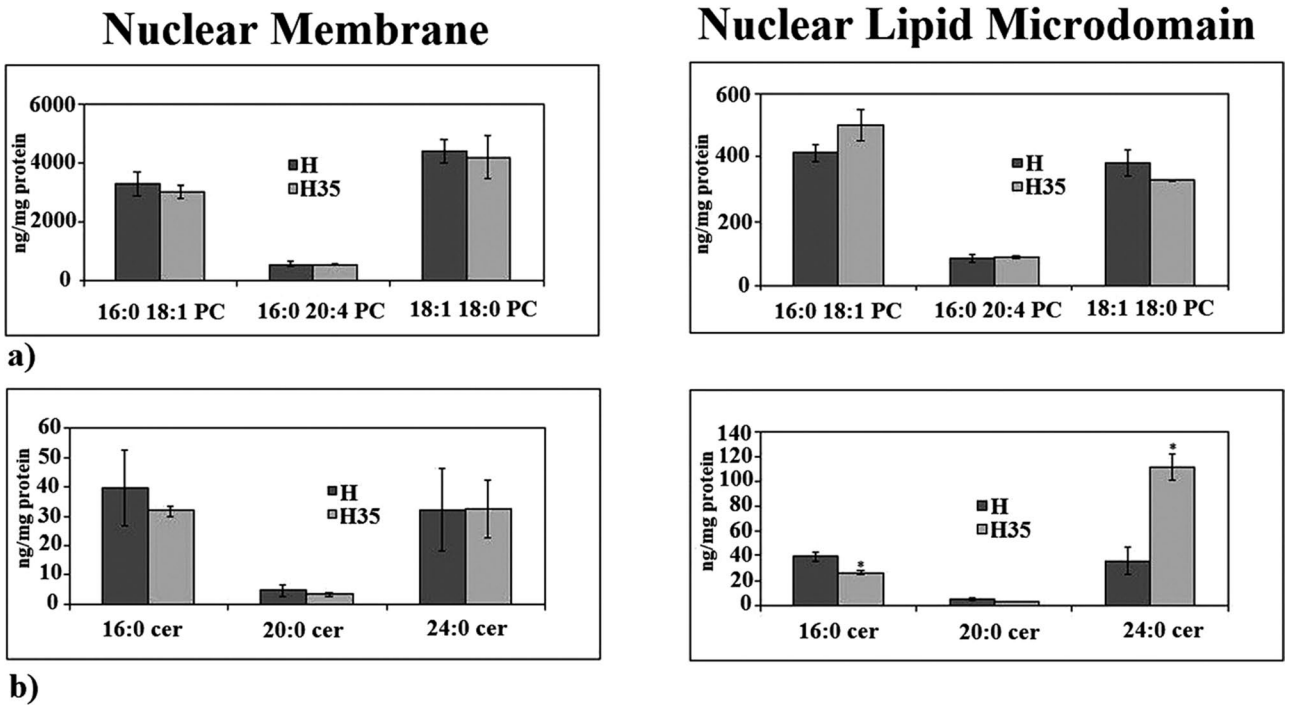

FIGURE 4: PC and ceramide in NM and NLMs purified from hepatocytes and hepatoma cells. (a) PC species studied by using 16:0 18:1 PC, 16:0 24:0 PC, and 18:1 18:0 PC external calibrators. (b) Ceramide species studied by using 16:0 ceramide, 20:0 ceramide, and 24:0 ceramide standards. Data are expressed as nmol/mg protein and represent the mean ± SD of three separate experiments. H, hepatocyte; H35, hepatoma cell line. *, $p < 0.001$ vs. H.

(Louie *et al.*, 2013). In addition, supplementation of culture medium with 16:0 modifies the FA composition of Reuber H35 hepatoma cells (Martínez-Cayuela *et al.*, 2000). The shift of sphingolipid composition from very long FAs (24:0) to long FAs (16:0) changes cell function (Sassa *et al.*, 2012).

We have demonstrated that NLMs act as a platform for duplication and transcription of active Chr (Cascianelli *et al.*, 2008; Albi *et al.*, 2013) and VDR (Bartoccini *et al.*, 2011), and as a site for dexamethasone regulation of gene expression (Cataldi *et al.*, 2014).

In this study, we demonstrated for the first time that, in NLMs of cancer cells, the FAs of SM change from very long FAs (24:0 SM) to long FAs (16:0 SM) in comparison with normal cells. Taking into account the calculated properties of 16:0 SM and 24:0 SM (van der Waals surface area and topological radius), it is possible to envisage that 24:0 SM is stronger than 16:0 SM in forming lipid microdomains with CHO. This hypothesis is supported by the larger van der Waals surface area of 24:0, which would allow a better accommodation of CHO underneath the polar headgroup of SM. It has been reported that SM forms bilayers with different thicknesses depending on the size of its FA chain, such as 46–47 Å for 18:0 SM and 52–56 Å for 24:0 SM (Maulik and Shipley, 1995, 1996). Comparing the topological diameters of 16:0 (33 Å), 18:0 (35 Å), 20:0 (37 Å), and 24:0 (41 Å) SM, the thickness of lipid rafts formed by 16:0 and 24:0 SM in combination with CHO can be in a range of 43–44 Å and 52–56 Å, respectively. In addition, our results indicate that H35 NLMs are enriched in unsaturated FAs, which is known to increase the area of a lipid and, consequently, membrane fluidity (Ziegelhöffer *et al.*, 2012). Rapidly growing evidence reinforces the notion that lipid rafts in membranes participate in the recruitment of proteins and lipid signaling molecules (Brown and London, 2000; Róg and Vattulainen, 2014). Therefore, considering our results, we hypothesize that the narrower thickness of NLMs composed of 16:0 SM and the increase of unsaturated FAs might determine enhanced dynamic properties of the NLRs in hepatoma cells, with an increased shuttling of protein molecules. We demonstrate here, in H35 NLMs, an increase of proteins involved in hepatocarcinogenesis, such as STAT3 (Hung *et al.*, 2014), Raf1 (Gauthier and Mitchell, 2013), and PKCζ (Desbois-Mouthon *et al.*, 2002) in spite of the reduction of VDR, probably for the reduction of vitamin D3, which inhibits hepatocellular carcinoma development (Guo *et al.*, 2013). The changes are higher in NLMs than in whole cells, supporting the idea that the modifications of NLMs in cancer cells might influence the content of functional proteins in these microdomains that act as platform for active Chr (Cascianelli *et al.*, 2008).

In conclusion, we show changes in SM and functional proteins of NLMs in cancer cells. This underlines the importance of focusing attention on NLMs instead of the global NM when cancer cells are studied.

MATERIALS AND METHODS

Animals and cells

Thirty-day-old Sprague Dawley rats of either sex (Harlan Nossan, Milan, Italy) kept at normal light–dark periods were used. They had free access to pelleted food and water before being killed between 9 and 10 a.m. All treatments were made according to the international regulations of the National Institutes of Health. H35 hepatoma cells were obtained from the European Collection of Animal Cell Cultures (Salisbury, UK).

Materials

DMEM, bovine serum albumin (BSA), dithiothreitol (DTT), fetal bovine serum (FBS), phenylmethylsulfonylfluoride (PMSF), methanol, 3-(4,5-dimethyl-thiazol-2-yl)-2,5-diphenyltetrazolium bromide, 2-propanol, metyl-tert-butyl ether, formic acid, chloroform, and CHO

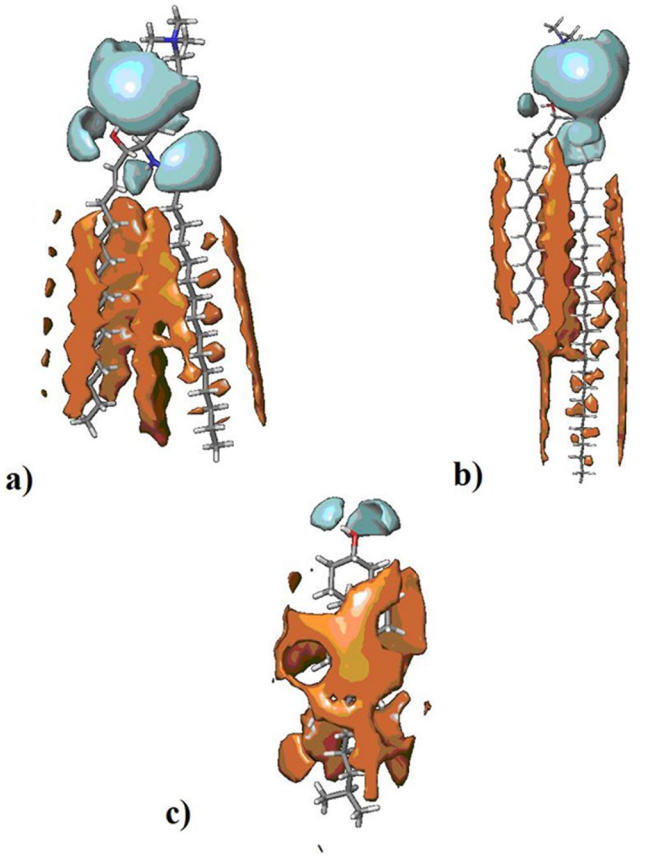

FIGURE 5: Models of 16:0 SM, 24:0 SM, and CHO. (a) Polar surface area (cyan) and lipophilic surface area (orange) of 16:0 SM. (b) Polar surface area (cyan) and lipophilic surface area (orange) of 24:0 SM. (c) Polar surface area (cyan) and lipophilic surface area (orange) of CHO.

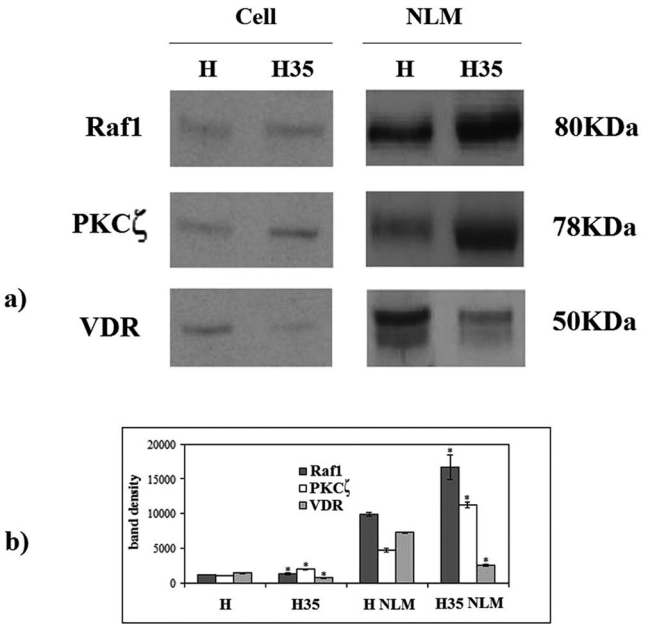

FIGURE 6: Raf1, PKCζ, and vitamin D3 receptor (VDR) in whole cells and in NLM purified from hepatocytes and hepatoma cells. (a) Immunoblot of proteins probed with specific antibodies, The position of proteins is indicated in relation to the position of molecular size standards. (b) The area density evaluated by densitometry scanning and analysis with Scion Image; the data represent the mean ± SD of three separate experiments. H, hepatocyte; H35, hepatoma cell line. *, $p < 0.001$ vs. H.

were obtained from Sigma-Aldrich (St. Louis, MO); lipid standards 16:0 SM, 18:1 SM, 24:0 SM, 16:0 18:1 PC, 16:0 24:0 PC, 18:1 18:0 PC, 16:0 ceramide, 20:0 ceramide, and 24:0 ceramide were purchased from Avanti (Avanti Polar, Alabaster, AL); anti-giantin, anti-STAT3, anti-Raf1, anti-PKCζ, and anti-VDR were obtained from Santa Cruz Biotechnology (Santa Cruz, CA); anti-lamin B was obtained from Oncogene (Boston, MA)

Rat liver

Rat liver was homogenized in 10 mM Tris-HCl buffer (pH 7.4) containing 0.25 M sucrose, 1 mM EDTA, 0.1% ethanol, 0.1 M PMSF, and 0.2 M DTT by using the Thomas homogenizer; the homogenate was filtered through two layers of surgical gauze and was used for hepatocyte nuclei isolation.

Cell culture

H35 hepatoma cells were seeded in 25 cm^2 flasks and were grown in monolayer in DMEM enriched with 10% FBS, 2 mM of L-glutamine, 100 IU/ml of penicillin, 100 µg/ml of streptomycin, and 250 µg/ml of amphotericin B. Cells were maintained at 37°C in a saturating humidity atmosphere containing 95% air, 5% CO_2 and were used for hepatoma nuclei isolation.

Hepatocyte and hepatoma cell nuclei isolation

H nuclei were isolated from liver homogenate according to Bresnick *et al.* (1967) in the presence of 1 mM PMSF, as previously described (Albi *et al.*, 1994). Briefly, liver homogenate was centrifuged at 700 × *g* for 10 min at 4°C. The procedure was repeated twice, and the final pellet was resuspended in 2.4 M sucrose containing 1 mM $MgCl_2$; this was followed by centrifugation at 50,000 × *g* for 60 min at 4°C. The pellet was washed with 0.25 M sucrose containing 1 mM MgCl2 and centrifuged at 2000 × *g* for 10 min. This method yielded a homogeneous population of hepatocyte nuclei with no contamination from other types of nuclei (Albi *et al.*, 1994).

H35 nuclei were isolated as previously reported (Albi *et al.*, 2005). Briefly, the homogenized cells were treated with 1% Triton X-100 in hypotonic buffer (0.5:1 vol/vol); the cellular suspension was stirred on a vortex mixer for 30 s; the buffer containing 1.5 M sucrose was added (0.25:1 vol/vol), and the solution was centrifuged at 2000 × *g* for 10 min.

The H and H35 cell nuclei were then washed twice with Barnes solution (0.085 M KCl, 0.0085 NaCl, 0.0025 M $MgCl_2$, 0.005 M trichloroacetic acid [TRA]-HCl), as previously reported (Rossi *et al.*, 2007). This treatment, during which the nuclei were sedimented at 2000 × *g*, removed mitochondrial and microsomal contaminations. The nuclei were checked for possible mitochondria and microsome contamination by evaluating the activity of a microsomal marker (NADH–cytochrome *c* reductase) and glucose-6-phosphatase, as previously reported (Albi *et al.*, 2005).

Purification of NM

NMs were purified from H and H35 isolated nuclei as previously reported (Albi *et al.*, 1997, 1999).

Purification of Chr

Chr was purified from H and H35 isolated nuclei as previously reported (Albi *et al.*, 2003b).

Purification of NMx

NMx was purified from H and H35 isolated nuclei as previously reported (Albi *et al.*, 2003a).

Purification of NLMs

NLMs were purified from H and H35 cell nuclei from normal and hepatectomized rats (Cascianelli *et al.*, 2008; Bartoccini *et al.*, 2011). The extraction was carried out with Triton X-100 dissolved in distilled water (10% vol/vol) on ice. This solution was added to the purified nuclei to a final detergent concentration of 1% (vol/vol). The extract was placed in a cushion of 80% sucrose with a gradient of 15–40% sucrose on top. After overnight centrifugation, floating fractions were carefully collected with a pipette, diluted five times with 25 mM HEPES-HCl, 150 mM NaCl (pH 7.1), and centrifuged at 100,000 × *g* for 120 min to obtain the pellet containing rafts. For testing the purity of NLRs, the absence of giantin, as a marker protein for Golgi membrane (Satoh *et al.*, 2005), and the presence of STAT3, as a specific NLR marker (Cascianelli *et al.*, 2008), were evaluated by immunoblot analysis.

Lipid extraction

Lipid extraction was performed according to Matyash *et al.* (2008) as reported by Lazzarini *et al.* (2014) with modifications. The pellets of H and H35 NLRs were suspended in Tris 10 mM, pH 7.4, and diluted with 1 ml methanol. Three milliliters ultra pure water and 3 ml MTBE were added. Each sample was vortexed for 1 min and centrifuged at 3000 × *g* for 5 min. The supernatant was recovered. The extraction with MTBE was repeated on the pellet and the supernatant was added to the first. The organic phase was dried under nitrogen flow and resuspended in 500 µl of methanol.

Ultrafast liquid chromatography–tandem mass spectrometry

The 16:0 SM, 18:1 SM, 24:0 SM, 16:0 18:1 PC, 16:0 24:0 PC, 18:1 18:0 PC, 16:0 ceramide, 20:0 ceramide, and 24:0 ceramide standards were prepared according to Matyash *et al.* (2008). Standards were dissolved in chloroform/methanol (9:1 vol/vol) at 10 µg/ml final concentration. The stock solutions were stored at –20°C. Working calibrators were prepared by diluting stock solutions with methanol to 500:0, 250:0, 100:0, and 50:0 ng/ml final concentrations. Twenty microliters of standards or lipids extracted from serum was injected after purification with specific nylon filters (0.2 µm)

Analyses were carried out according to Rabagny *et al.* (2011) by using the Ultra Performance Liquid Chromatography system tandem mass spectrometer (Applied Biosystems, Italy). The lipid species were separated, identified, and analyzed as previously reported (Garcia-Gil *et al.*, 2014). The samples were separated on a Phenomenex Kinetex phenyl-hexyl 100 A column (50 × 4.60-mm diameter, 2.6-µm particle diameter) with a precolumn security guard Phenomenex ULTRA phenyl-hexyl 4.6. For SM, column temperature was set at 50°C and flow rate at 0.9 ml/min. Solvent A was 1% formic acid; solvent B was 100% isopropanol containing 0.1% formic acid. The run was performed for 3 min in 50% solvent B and then in a gradient to reach 100% solvent B in 5 min. The system needed to be reconditioned for 5 min with 50% solvent B before the next injection. The SM species were identified by using positive turbo-ion spray and modality multipole-reaction monitoring. The identification and analysis of CHO was conducted by atmospheric pressure chemical ionization in positive ionization conditions and multipole-ion scan modality.

Protein content

Total protein concentration was determined spectrophotometrically at 750 nm by using bovine BSA as a standard, as previously reported (Albi *et al.*, 2008).

Electrophoresis and Western blot analysis

Thirty micrograms of protein from H and H35 NLRs was submitted to SDS–PAGE electrophoresis in an 8% polyacrylamide slab gel for giantin detection and a 10% gel for STAT3, Raf1, PKCζ, VDR, and lamin B according to Laemmli (1970). For the electrophoresis image analysis, the gel was stained with Coomassie blue. The transfer of protein was carried out onto nitrocellulose in 90 min according to Towbin *et al.* (1979). The membranes were blocked for 30 min with 5% nonfat dry milk in PBS (pH 7.5) and incubated overnight at 4°C with specific antibodies. The blots were treated with horseradish-conjugated secondary antibodies for 90 min. Visualization was performed with the enhanced chemiluminescence kit from Amersham Pharmacia Biotech (Rainham, Essex, UK).

Properties of 16:0 SM, 24:0 SM, and CHO

Three-dimensional chemical structures of 16:0 SM, 24:0 SM, and CHO were generated using Maestro v9.5 (Schrödinger, NY). Geometries were optimized using semiempirical calculations with AM1 method and RHF wavefunction. Surface and geometrical properties, including polar surface area (Å^2), total van der Waals surface area (Å^2), topological radius (Å), and topological diameter (Å), were calculated using Canvas v1.7 (Schrödinger, NY).

Statistical analysis

Data are expressed as mean ± SD, and a *t* test was used for statistical analysis.

REFERENCES

Adan-Gokbulut A, Kartal-Yandim M, Iskender G, Baran Y (2013). Novel agents targeting bioactive sphingolipids for the treatment of cancer. Curr Med Chem 20, 108–122.

Aittoniemi J, Niemela PS, Hyvonen MT, Karttunen M, Vattulainen I (2007). Insight into the putative specific interactions between cholesterol, sphingomyelin, and palmitoyl-oleoyl phosphatidylcholine. Biophys J 92, 1125–1137.

Albi E, Cataldi S, Rossi G, Magni MV (2003a). A possible role of cholesterol-sphingomyelin/phosphatidylcholine in nuclear matrix during rat liver regeneration. J Hepatol 38, 623–628.

Albi E, La Porta CA, Cataldi S, Magni MV (2005). Nuclear sphingomyelin-synthase and protein kinase C delta in melanoma cells. Arch Biochem Biophys 438, 156–161.

Albi E, Lazzarini A, Lazzarini R, Floridi A, Damaskopoulou E, Curcio F, Cataldi S (2013). Nuclear lipid microdomain as place of interaction between sphingomyelin and DNA during liver regeneration. Int J Mol Sci 14, 6529–6541.

Albi E, Lazzarini R, Viola Magni M (2008). Phosphatidylcholine/sphingomyelin metabolism crosstalk inside the nucleus. Biochem J 410, 381–389.

Albi E, Mersel M, Leray C, Tomassoni ML, Viola-Magni MP (1994). Rat liver chromatin phospholipids. Lipids 29, 715–719.

Albi E, Peloso I, Magni MV (1999). Nuclear membrane sphingomyelin-cholesterol changes in rat liver after hepatectomy. Biochem Biophys Res Commun 262, 692–695.

Albi E, Pieroni S, Viola Magni MP, Sartori C (2003b). Chromatin sphingomyelin changes in cell proliferation and/or apoptosis induced by ciprofibrate. J Cell Physiol 196, 354–361.

Albi E, Tomassoni ML, Viola-Magni M (1997). Effect of lipid composition on rat liver nuclear membrane fluidity. Cell Biochem Funct 15, 181–190.

Albi E, Villani M (2009). Nuclear lipid microdomains regulate cell function. Commun Integr Biol 2, 23–24.

Bartoccini E, Marini F, Damaskopoulou E, Lazzarini R, Cataldi S, Cascianelli G, Garcia-Gil M, Albi E (2011). Nuclear lipid microdomains regulate nuclear vitamin D3 uptake and influence embryonic hippocampal cell differentiation. Mol Biol Cell 22, 3022–3031.

Bresnick E, Lanclos K, Sage J, Schwartz A, Yawn DH, Bush H, Hunuma T (1967). Isolation and ribonucleic acid synthesis in nuclei of rat fetal liver. Exp Cell Res 46, 396–411.

Brown DA (2006). Lipid rafts, detergent-resistant membranes, and raft targeting signals. Physiol 21, 430–439.

Brown DA, London E (2000). Structure and function of sphingolipid- and cholesterol-rich membrane rafts. J Biol Chem 275, 17221–17224.

Cascianelli G, Villani M, Tosti M, Marini F, Bartoccini E, Magni MV, Albi E (2008). Lipid microdomains in cell nucleus. Mol Biol Cell 19, 5289–5295.
Cataldi S, Codini M, Cascianelli G, Tringali S, Tringali AR, Lazzarini A, Floridi A, Bartoccini E, Garcia-Gil M, Lazzarini R, *et al*. (2014). Nuclear lipid microdomain as resting place of dexamethasone to impair cell proliferation. Int J Mol Sci 15, 9832–9846.
Desbois-Mouthon C, Blivet-Van Eggelpoël MJ, Beurel E, Boissan M, Delélo R, Cadoret A, Capeau J (2002). Dysregulation of glycogen synthase kinase-3β signaling in hepatocellular carcinoma cells. Hepatology 36, 1528–1536.
Frisz JF, Klitzing HA, Lou K, Hutcheon ID, Weber PK, Zimmerberg J, Kraft ML (2013). Sphingolipid domains in the plasma membranes of fibroblasts are not enriched with cholesterol. J Biol Chem 288, 16855–16861.
Garcia-Gil M, Lazzarini A, Lazzarini R, Floridi E, Cataldi S, Floridi A, Albi E (2014). Serum deprivation alters lipid profile in HN9.10e embryonic hippocampal cells. Neurosci Lett 589, 83–87.
Gauthier A, Mitchell H (2013). The role of sorafenib in the treatment of advanced hepatocellular carcinoma: an update. Hepatol Res 43, 147–154.
Guo J, Ma Z, Ma Q, Wu Z, Fan P, Zhou X, Chen L, Zhou S, Goltzman D, Miao D, Wu E (2013). 1, 25$(OH)_2D_3$ inhibits hepatocellular carcinoma development through reducing secretion of inflammatory cytokines from immunocytes. Curr Med Chem 20, 4131–4141.
Holopainen JM, Metso AJ, Mattila JP, Jutila A, Kinnunen PK (2004). Evidence for the lack of a specific interaction between cholesterol and sphingomyelin. Biophys J 86, 1510–1520.
Honigmann A, Mueller V, Ta H, Schoenle A, Sezgin E, Hell SW, Eggeling C (2014). Scanning STED-FCS reveals spatiotemporal heterogeneity of lipid interaction in the plasma membrane of living cells. Nat Commun 5, 5412.
Hung MH, Tai WT, Shiau CW, Chen KF (2014). Downregulation of signal transducer and activator of transcription 3 by sorafenib: a novel mechanism for hepatocellular carcinoma therapy. World J Gastroenterol 20, 15269–15274.
Laemmli UK (1970). Cleavage of structure proteins during the assembly of bacteriophage T4. Nature 227, 680–683.
Lazzarini A, Floridi A, Pugliese L, Villani M, Cataldi S, Codini M, Lazzarini R, Beccari T, Ambesi-Impiombato FS, Curcio F, Albi E (2014). Analysis of serum sphingomyelin species by UFLC-MS/MS in patients affected with monoclonal gammopathy. J Chromat Separation Techniq 5, 1000239.
Levin IW, Thompson TE, Barenholz Y, Huang C (1985). Two types of hydrocarbon chain interdigitation in sphingomyelin bilayers. Biochemistry 24, 6282–6286.
Li XM, Momsen MM, Smaby JM, Brockman HL, Brown RE (2001). Cholesterol decreases the interfacial elasticity and detergent solubility of sphingomyelins. Biochemistry 40, 5954–5963.
Louie SM, Roberts LS, Mulvihill MM, Luo K, Nomura DK (2013). Cancer cells incorporate and remodel exogenous palmitate into structural and oncogenic signaling lipids. Biochim Biophys Acta 1831, 1566–1572.
Martínez-Cayuela M, García-Pelayo MC, Linares A, García-Peregrín E (2000). Metabolism of palmitic and docosahexaenoic acids in Reuber H35 hepatoma cells. J Biochem 128, 545–551.
Matyash V, Liebisch G, Kurzchalia TV, Shevchenko A, Schwudke D (2008). Lipid extraction by methyl-tert-butyl ether for high-throughput lipidomics. J Lipid Res 49, 1137–1146.
Maulik PR, Shipley GG (1995). X-ray diffraction and calorimetric study of *N*-lignoceryl sphingomyelin membranes. Biophys J 69, 1909–1916.
Maulik PR, Shipley GG (1996). Interactions of *N*-stearoyl sphingomyelin with cholesterol and dipalmitoylphosphatidylcholine in bilayer membranes. Biophys J 70, 2256–2265.
Mollinedo F, Gajate C (2015). Lipid rafts as major platforms for signaling regulation in cancer. Adv Biol Regul 57, 130–146.
Ohno Y, Suto S, Yamanaka M, Mizutani Y, Mitsutake S, Igarashi Y, Sassa T, Kihara A (2010). ELOVL1 production of C24 acyl-CoAs is linked to C24 sphingolipid synthesis. Proc Natl Acad Sci USA 107, 18439–18444.
Rabagny Y, Herrmann W, Geisel J, Kirsch SH, Obeid R (2011). Quantification of plasma phospholipids by ultra performance liquid chromatography tandem mass spectrometry. Anal Bioanal Chem 401, 891–899.
Radhakrishnan A, Anderson TG, McConnell HM (2000). Condensed complexes, rafts, and the chemical activity of cholesterol in membranes. Proc Natl Acad Sci USA 97, 12422–12427.
Róg T, Pasenkiewicz-Gierula M (2006). Cholesterol–sphingomyelin interactions: a molecular dynamics simulation study. Biophys J 91, 3756–3767.
Róg T, Vattulainen I (2014). Cholesterol, sphingolipids, and glycolipids: what do we know about their role in raft-like membranes? Chem Phys Lipids 184, 82–104.
Rossi G, Magni MV, Albi E (2007). Sphingomyelin-cholesterol and double stranded RNA relationship in the intranuclear complex. Arch Biochem Biophys 459, 27–32.
Sassa T, Suto S, Okayasu Y, Kihara A (2012). A shift in sphingolipid composition from C24 to C16 increases susceptibility to apoptosis in HeLa cells. Biochim Biophys Acta 1821, 1031–1037.
Satoh A, Beard M, Warren G (2005). Preparation and characterization of recombinant golgin tethers. Methods Enzymol 404, 279–296.
Slotte JP (2013a). Molecular properties of various structurally defined sphingomyelins—correlation of structure with function. Prog Lipid Res 52, 206–219.
Slotte JP (2013b). Biological functions of sphingomyelins. Prog Lipid Res 52, 424–437.
Soupene E, Kuypers FA (2008). Mammalian long-chain acyl-CoA synthetases. Exp Biol Med 233, 507–521.
Taniguchi M, Okazaki T (2014). The role of sphingomyelin and sphingomyelin synthases in cell death, proliferation and migration—from cell and animal models to human disorders. Biochim Biophys Acta 1841, 692–703.
Todeschini R, Consonni V (2000). Handbook of Molecular Descriptors, Methods and Principles in Medicinal Chemistry 11, Weinheim, Germany: Wiley-VCH, 366–510.
Towbin H, Staehelin T, Gordon J (1979). Electrophoretic transfer of proteins from polyacrylamide gels to nitrocellulose sheets: procedure and some applications. Proc Natl Acad Sci USA 76, 4350–4354.
Zhang L, Ji J, Zhu XY, Wu YY, Yu H, Zhang B, Li XL, Sun XZ (2004). Palmitic acid induces apoptosis in human hepatoma cell line, HepG2 cells. Zhongguo Yi Xue Ke Xue Yuan Xue Bao 26, 671–676.
Ziegelhöffer A, Waczulíková I, Ferko M, Šikurová L, Mujkošová J, Ravingerová T (2012). Involvement of membrane fluidity in endogenous protective processes running on subcellular membrane systems of the rat heart. Physiol Res 61(Suppl 2), S11–S21.